

Disorder in Al-Li-Cu and Al-Mn-Si Icosahedral Alloys

P. A. HEINEY, P. A. BANCEL, P. M. HORN, J. L. JORDAN, S. LAPLACA, J. ANGILELLO, F. W. GAYLE

Faceted dendrites of icosahedral $\text{Al}_6\text{Li}_3\text{Cu}$ have been studied by high-resolution x-ray scattering. The samples display long-range icosahedral symmetry both in their diffraction patterns and in their macroscopic morphology. Despite the appearance of well-defined facets, the samples have a high degree of atomic disorder. The Bragg peaks have symmetry-dependent shapes and widths that scale linearly with G_{\perp} (phason momentum). The peak widths are surprisingly similar to those found in icosahedral Al-Mn-Si alloys in both their absolute magnitude and their dependence on G_{\perp} . The origin of these features in models for the icosahedral phase is discussed.

SINCE THE DISCOVERY (1) OF ICOSAHEDRAL alloys, several approaches have been used to elucidate their structure. Theoretical efforts have focused on the wide variety of distinct quasiperiodic tiling (2) and projection (3) algorithms that can yield long-range icosahedral order, as well as on the building of atomic models (4) and on the crystallography of quasiperiodic structures (5). Much progress has been made in understanding icosahedral quasilattices (4–7), but there is still no agreement about which decorations might correctly describe atomic positions.

In this report we focus on the defect structure of these materials. X-ray scattering experiments (8–10) have shown that diffraction peaks in icosahedral alloys are broad, which indicates the presence of substantial disorder. As shown below, diffraction peaks in icosahedral Al-Li-Cu display a variety of line shapes that cannot be attributed to any simple mechanism such as the presence of impurity phases or conventional defects, which suggests that an unusual type of disorder is involved. Furthermore, the radial peak widths are remarkably similar to those found in icosahedral Al-Mn-Si alloys in both their absolute magnitude and their dependence on phason momentum (9, 11–13), which suggests a common origin for the disorder in this class of icosahedral materials.

In ordinary, commensurate materials, the peak broadening due to strain fields from defects increases monotonically with the magnitude of the reciprocal lattice vector $|\mathbf{G}|$. Although the details of the defect distribution can give symmetry dependence to the broadening, widths of peaks of a given

symmetry generally increase monotonically with increasing wave vector. As discussed below, the peak widths in icosahedral alloys, even for peaks of the same symmetry, do not show this simple dependence on $|\mathbf{G}|$. The widths and line shapes of icosahedral-phase x-ray peaks are associated with disorder in the phason variable, which enters into the description of icosahedral systems as a consequence of their incommensurability (9, 12) (Fig. 1). In quasicrystalline models, phason strains can couple to a conjugate variable \mathbf{G}_{\perp} just as strains in the atomic density couple to the momentum transfer \mathbf{G} and can generate a \mathbf{G}_{\perp} dependence of peak widths and shapes in diffraction data. An alternate approach to understanding icosahedral alloys is given by the random-packing models (14, 15), which describe the structures as the orientationally ordered accretion of icosahedral clusters. However, these models predict that phason disorder also enters in a natural way. Indeed, the simplest random packings introduce disorder in the phason variable alone. An important unresolved question in the study of icosahedral structures is whether the random-packing models, which emphasize disorder, or defected quasicrystal models, which emphasize quasiperiodic translational order, provide a more accurate description of the experimentally studied alloys. The details of the disorder allowed within each model can be compared with experimentally observed disorder.

Detailed studies of disorder have been hindered by the small grain size of the rapidly quenched alloys, which has restricted high-resolution x-ray scattering studies to powder samples and has made careful measurements of line shapes difficult. The recent discovery that Al-Li-Cu alloys can form very large icosahedral grains (16, 17) has removed this restriction; in this report we present high-resolution x-ray scattering data from large faceted single grains of an icosahedral alloy (18). Details of sample prepara-

tion have been presented elsewhere (17). Briefly, $\text{Al}_6\text{Li}_3\text{Cu}$ was cast from a stoichiometric charge and solidified within the crucible used for melting (19). The charge was slowly cooled at approximately 9°C per minute below a thermal arrest temperature of 623°C . The bulk T_2 phase (20), which we identify as the icosahedral phase, solidified into large grains (1 to 3 mm in diameter) surrounded by eutectic. X-ray powder scans showed that the eutectic contained a variety of crystalline phases: face-centered cubic aluminum and the large-unit-cell $T_1(\text{Al}_2\text{CuLi})$ (20) and $R(\text{Al}_5\text{CuLi}_3)$ (21) phases. The single grains used in this study grew as faceted dendrites into shrink cavities within the bulk of a slowly cooled alloy (19). The dendrites grew along their fivefold symmetry axes; their orientations are often correlated. The most perfect dendrites are capped with five symmetrically arranged rhombohedral faces (Fig. 2). The length ratio of the

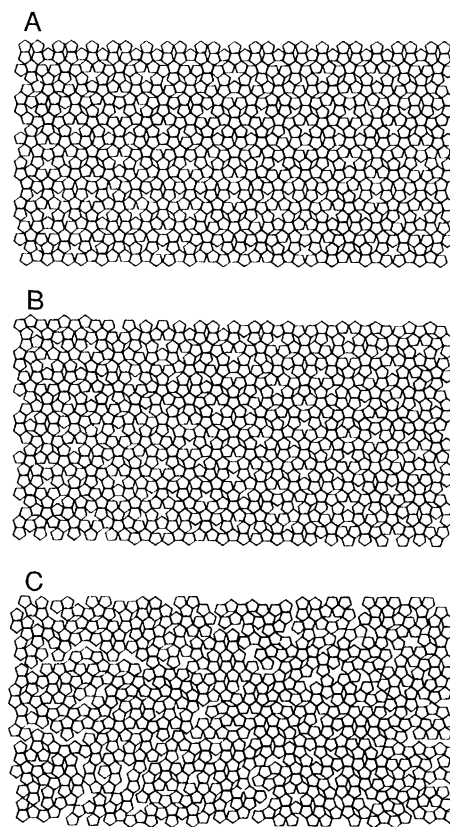
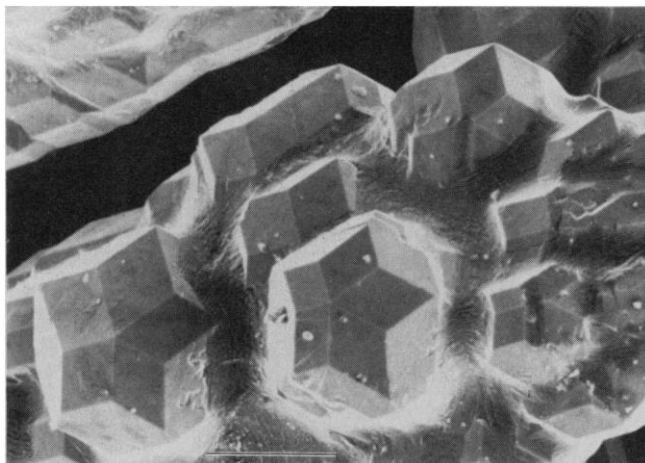


Fig. 1. (A) A quasicrystalline array composed of pentagons, stars, and slivers. The diffraction pattern from this structure would yield perfect Bragg peaks similar to those from a Penrose tiling. (B) A linear phason strain has been imposed on the structure from (A). (C) A random packing of pentagons. This structure can formally be represented as a quasicrystalline array modified by a high density of random phason strains. Differences between the patterns are best observed by viewing them at a glancing angle; the quasiperiodically spaced rows of edges in (A) acquire “jogs” in (B) and become wavy and disordered in (C). [Figure courtesy of P. W. Stephens]

P. A. Heiney and P. A. Bancel, Department of Physics and Laboratory for Research on the Structure of Matter, University of Pennsylvania, Philadelphia, PA 19104.
P. M. Horn, J. L. Jordan, S. LaPlaca, J. Angilello, IBM T. J. Watson Research Center, Yorktown Heights, NY 10598.
F. W. Gayle, Metallurgy Laboratory, Reynolds Metals Company, P.O. Box 27003, Richmond, VA 23261.

Fig. 2. Scanning electron micrograph that shows the growth habit of icosahedral dendrites of $\text{Al}_6\text{Li}_3\text{Cu}$. The rhombohedral facets are about $50\ \mu\text{m}$ on a side. The eutectic is visible at the base of the dendrite arms.



major and minor axes of the rhombi appears to be equal to the golden mean, $\tau = (1 + \sqrt{5})/2$. These caps are well approximated as portions of a rhombic triacontahedron (Fig. 3), a convex solid with 30 “golden rhombus” faces and 60 edges that connect threefold vertices to fivefold vertices. In the scattering experiment, single crystals of the type shown in Fig. 2 mounted on a glass fiber. The samples were approximately 0.1 to 0.3 mm in size and consisted of one major dendrite arm with numerous triacontahedral side branches.

The macroscopic morphology of crystals is often directly related to the symmetry and packing of local microscopic units. Indeed, historically this observation led to the first suggestion that crystals are composed of identical microscopic unit cells (22). Neumann’s principle states that the macroscopic symmetry elements of a freely growing faceted crystal must include the symmetry of the crystal point group (23). A triacontahedron has the $\bar{m}35$ symmetry of an icosahedron; unit cells of icosahedral symmetry cannot pack in a periodic manner and maintain macroscopic triacontahedral symmetry. Nevertheless, diffraction from Al-Li-Cu displays an icosahedral point symmetry. In Fig. 4 we plot x-ray intensity versus momentum transfer for radial scans in \mathbf{G} through two Bragg peaks (24, 25). The momentum transfer is defined as $|\mathbf{G}| = (4\pi/\lambda)\sin\theta$, where λ is the wavelength of the incoming x-rays and θ is the scattering angle. The peaks have been indexed with the six-index vertex vector notation (8). We use the convention in which the basis vectors are given by cyclic permutations of $q_0(1, \pm\tau, 0)$, where q_0 defines the scale of the reciprocal lattice. The scans have been fitted to Gaussians or sums of Gaussians (solid lines), which provide a useful parametrization of the line widths, although they do not completely describe the shapes of the peaks.

A number of results are immediately clear.

First, the peaks are much broader than the instrumental resolution, which indicates the presence of considerable disorder. The radial peak widths vary from 0.005 to $0.04\ \text{\AA}^{-1}$ half-width at half-maximum (HWHM). Second, transverse scans through these peaks are also quite broad. The transverse widths of these peaks, which can be as large as 2.5° ($0.04\ \text{\AA}^{-1}$) for the $1(\bar{1}12200)$ peak, cannot be simply attributed to misoriented subgrains (mosaic blocks), because symmetry equivalent peak widths decrease for larger scattering angles. Third, peaks with different symmetries have different line shapes. For example, radial scans through vertex symmetry peaks [that is, peaks whose associated reciprocal lattice vectors intersect the vertices of an icosahedron, such as the (100000)], are bimodal, whereas peaks of other symmetries are relatively structureless. The striking bimodal character of the vertex peaks cannot be explained by compositional modulations (variations in the lattice constant) in the sample, since this splitting is not displayed by other peaks, such as the nearby (110000) .

The peak widths for Al-Li-Cu, as well as other icosahedral alloys that have been studied, do not scale monotonically with $|\mathbf{G}|$. However, the peak widths do have a nearly linear dependence on G_\perp . Figure 5A shows a plot of peak HWHM for radial scans through all of the peaks measured on one of the dendritic $\text{Al}_6\text{Li}_3\text{Cu}$ samples. A straight line passing through the origin provides a

reasonable fit to the data, as would be expected if the disorder were purely G_\perp -dependent. Analysis of data from a second sample results in a similar fit but with a different slope. We can understand the observed variation of peak width with G_\perp by assuming that the defect structure of dendritic Al-Li-Cu can be characterized by anisotropic linear phason strains. Such strains lead to shifts in peak position (11–13) given by $\Delta\mathbf{G} = \mathbf{M}\mathbf{G}_\perp$, where \mathbf{M} is a matrix that describes a linear phason strain field. A distribution of such strains in the sample can be described by assigning different values of \mathbf{M} to different regions of the sample. Each region can be considered as a coherent “domain” that contributes Bragg scattering into a reciprocal lattice point $\mathbf{G}_{\text{Bragg}} + \mathbf{M}\mathbf{G}_\perp$. Thus the measured intensity about any reciprocal lattice point will correspond to an ensemble of peaks from all such domains as determined by the matrices $\{\mathbf{M}\}$.

In general, a random distribution of strains will give many overlapping peaks and result in a broad, smooth scattered intensity maximum. However, effects due to growth kinetics or local energy considerations can restrict or skew the distribution of $\{\mathbf{M}\}$ and result in a restricted set of diffraction peaks in the ensemble. Electron microscopy observations of electron diffraction from rapidly quenched Al-Li-Cu ribbons show that phasonlike peak shifts are perpendicular to the dendrite growth directions, which suggests that the distribution of $\{\mathbf{M}\}$ is influenced by the direction of sample growth; this effect has also been seen in rapidly quenched Al-Mn alloys (26). The samples used in the present study were cooled relatively slowly rather than being melt-spun. However, phason disorder may correlate with the growth direction, since these samples also grow dendritically and x-ray powder diffraction scans of both slowly and rapidly quenched Al-Li-Cu powders show nearly identical peak widths and shapes.

Thus the diffraction peak widths and shapes in Al-Li-Cu are consistent with a model in which the predominant defects can be described in terms of anisotropic linear phason strains, which are correlated with the growth direction. The model provides a unified picture of the scattering data, includ-

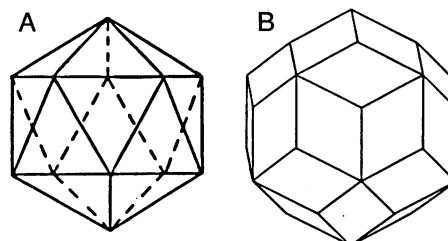
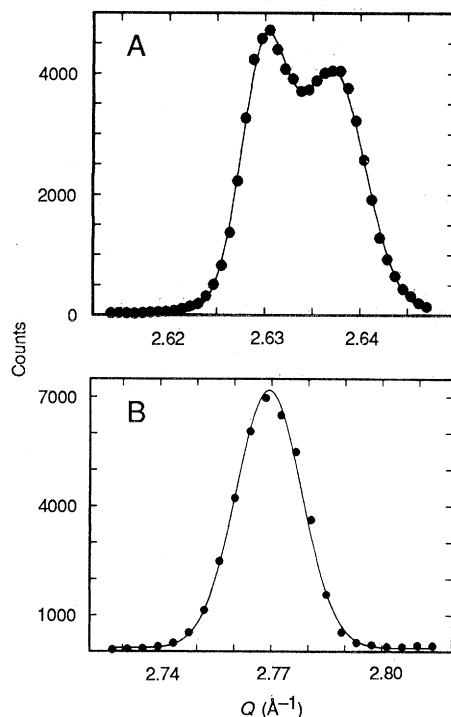


Fig. 3. (A) An icosahedron and (B) a rhombic triacontahedron. The triacontahedron can be constructed by replacing the edges of the icosahedron with rhombic faces.

Fig. 4. Scattered intensity versus momentum transfer for radial scans through the (A) (100000) (vertex) and (B) (110000) (edge) Bragg peaks. Solid lines are fits to Gaussian line shapes. Vertical axis measures photons counted per 20,000 counts in a monitor detector placed before the sample.



ing the following features: First, the scattering in the vicinity of a Bragg peak, $\mathbf{G}_{\text{Bragg}}$, will be comprised of an ensemble of peaks given by $\mathbf{G} = \mathbf{G}_{\text{Bragg}} + \mathbf{M}\mathbf{G}_{\perp}$, where $\{\mathbf{M}\}$ describes a restricted distribution of phason strains in the sample. Second, peaks of the same symmetry will have the same shape, as in fact observed in the data. For example, all vertex peaks have the same line shape, with a bimodal splitting in the radial direction. Third, the spread in reciprocal space of ensembles of peaks will vary linearly with \mathbf{G}_{\perp} (Fig. 5A). This gives rise to the \mathbf{G}_{\perp} dependence of the measured peak widths. (Note that, for the split vertex peaks, the width here refers to the extent of the entire peak structure, rather than that of any individual peak included in the cluster.) The possibility that the alloys lock into a commensurate phase remains but is unlikely since we measure different magnitudes of strain in different samples (that is, different slopes in the fits to different samples). A complete description of peak shifts and broadening must include symmetry-dependent effects. A description of peak shifts and broadenings in terms of anisotropic linear phason strains has recently been developed by Socolar and Wright (27). By incorporating linear phason strain associated with growth anisotropy, they account for x-ray peak shapes and shifts in both Al-Li-Cu and Al-Mn-Si samples and also the shapes of spots seen in electron diffraction patterns.

Individual peaks in an ensemble can also be broadened by other effects such as finite grain size, sample mosaic (which broadens peaks in the transverse directions only),

conventional \mathbf{G} -dependent strains, variations in the magnitudes of $\{\mathbf{M}\}$, or nonlinear components of the phason strain. In fact, a crossover to \mathbf{G} -dependence (or finite size broadening) is seen in the low \mathbf{G}_{\perp} (high \mathbf{G}) end of the edge-series peaks (see Fig. 5A). These effects in addition to the three-dimensional instrumental-resolution function will smear out the ensemble of peaks about each Bragg reflection. However, the vertex peaks (Fig. 4) have considerable structure. (Careful measurements of the three-dimensional structure of these peaks indicate the presence of other maxima in the scattering function in addition to the two major peaks shown, which are split in the radial direction. Also, the two major peaks do not always have the same amplitude.) If we describe the vertex peak profiles as the sum of two Gaussian line shapes, we can extract an estimate for the widths of individual peaks in the ensemble; we find a peak width of 0.0025 \AA^{-1} (HWHM) for the (100000). The peak width is consistent with an effective crystallite size of $\pi/0.0025 \text{ \AA}^{-1} = 1250 \text{ \AA}$.

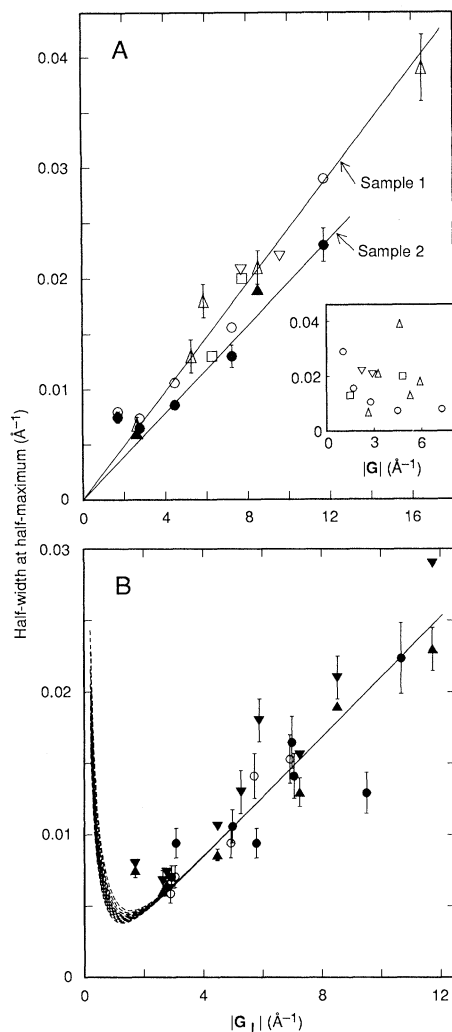
We now discuss the magnitude of the peak widths. A striking feature of our results is the similarity between Al-Li-Cu and Al-Mn-Si. In Fig. 5B we replot the width of edge symmetry Bragg peaks versus phason momentum for our Al-Li-Cu samples and for film-deposited, annealed Al-Mn-Si. The solid lines represent the peak widths theoretically predicted by Horn *et al.* for dislocation disorder (9), which for icosahedral materials incorporates both phonon and phason strains. Although all the points do not fit

exactly on the same curve, the peak widths for a given $|\mathbf{G}_{\perp}|$ all agree within a factor of 2. It is difficult to justify a priori that single crystals of Al-Li-Cu should have quantitatively the same strains as icosahedral films of Al-Mn-Si. Neither the Bragg peak intensities nor the local structures of the two materials are similar (4). Despite some differences in shape, the Bragg peak widths are quantitatively similar, and do not appear to depend sensitively on either sample composition or growth rate. Spin-condensed ribbons of Al-Li-Cu as well as annealed spin-condensed ribbons of Al-Mn-Si have qualitatively similar peak widths (7-10), although these samples were cooled orders of magnitude more rapidly than our Al-Li-Cu samples. (However, it should be noted that it is difficult to unambiguously relate the rate at which the entire sample was cooled to the velocity of the growth front; we estimate a ratio of 100 to 1000 between the growth rates in the two types of sample). Thus the data suggest that phason disorder of a specific magnitude is a universal feature of this class of alloy.

One approach to understanding the universal phason disorder can be found in accretion models for the growth of the icosahedral phase. In these models, local icosahedral units are accreted by the attachment of an icosahedron to a randomly chosen vertex (14) or face (15) of an icosahedral seed. To ensure orientational order, adjacent icosahedra are given the same orientation. The resulting structure is highly disordered and yet has macroscopic orientational order. Because the disorder is primarily of phason character, the predicted Bragg peaks are quite sharp and have widths that increase monotonically with $|\mathbf{G}_{\perp}|$. However, the model in its simplest form cannot be correct in detail; it contains random strains that cause an isotropic $|\mathbf{G}_{\perp}|^2$ dependence (9) of the width, whereas the data on Al-Li-Cu indicate an anisotropic, linear dependence. A linear component to the phason strain can be incorporated by allowing anisotropic random packing of the icosahedral structural units (28); the quadratic component of the phason strain (and associated "tears" in the structure) can be further removed by allowing a certain amount of thermal relaxation in the growth algorithm (29). Indeed, as farther-neighbor interactions are added, the generated structure approaches that of a true quasicrystal. Conversely, if a phason strain is added to a quasiperiodic tiling a certain density of matching-rule violations (13) result, which can be interpreted as places where the structural units fit together in an energetically unfavorable way.

In either the icosahedral glass or the quasicrystal models the presence of phason

Fig. 5. (A) Peak half-width at half-maximum versus phason momentum. Solid lines indicate least-squares lines. Symbols identify peak symmetries (open symbols for sample 1, solid for sample 2). The indices for the peaks, in order of increasing $|G_{\perp}|$ are: vertex (Δ, \blacktriangle): (100000), (200000), (011111), (111111), and (411111); edge (\circ, \bullet): (112200), (111100), (001100), (110000), and (111100); face (\square): (110001) and (111111); other (∇): (121010), (111101). Except where noted the size of the plotted points represents the estimated uncertainty in the peak widths. Uncertainties in the width were obtained by systematic variations of all parameters in least-squares fits. The scatter in measured peak widths around the least-squares line is greater than the estimated error; these deviations are reproducible and result either from true deviations from ideal linear phason strain or from shifts due to the inadequacy of the Gaussian parameterization of the peaks. In the inset the peak HWHM for sample 1 is plotted versus $|G_{\perp}|$. (B) Peak widths versus phason momentum from two $\text{Al}_6\text{Li}_3\text{Cu}$ samples (triangles) and two Al-Mn-Si samples (circles). The peak widths are Gaussian half-widths obtained from theoretical fits. The solid line through the data represents the phason-disorder model of Horn *et al.* with 2000 Å between dislocations (9). The model uses estimates for the elastic constants of Al-Mn-Si by Sachdev and Nelson (33) and Jarić (34).



strains may represent defects in the way structural units are arranged; the fact that the strains are primarily anisotropic and are associated with the growth direction suggests that the defects are introduced by "incorrect attachments" of structural units during the growth process. In these models, the magnitude of phason strain is proportional to the probability of a misattachment multiplied by the size of a structural unit. (This is comparable to saying that in ordinary crystals the strain due to dislocations is proportional to the density of dislocations multiplied by the length of a Burger's vector, which is determined by the size of the unit cell.) As pointed out by Levine *et al.* (30), phasons represent overdamped hydrodynamic modes and hence cannot easily be removed. Thus the phason disorder remains in the sample regardless of the equilibrium state of the material or the annealing time of the specific sample. In contrast, normal "phonon" (compressive or shear)-type strains are expected to self-anneal at a rate comparable to that in normal crystals.

Although this report has emphasized the implications of the x-ray line broadening,

the observation of faceted icosahedral dendrites also has intriguing consequences. For example, faceting is expected in the equilibrium growth of icosahedral quasicrystals (31) and persists even in the presence of substantial disorder (32). Our observation should stimulate investigation into the growth habit implied by other models for the icosahedral phase.

REFERENCES AND NOTES

- D. Shechtman, I. Blech, D. Gratias, J. W. Cahn, *Phys. Rev. Lett.* **53**, 1951 (1984).
- D. Levine and P. J. Steinhardt, *ibid.*, p. 2477.
- M. Duneau and A. Katz, *ibid.*, p. 2688; V. Elser, *Phys. Rev. B* **32**, 4892 (1985); see also papers from the *International Workshop on Aperiodic Crystals* [*J. Phys. (Paris)* **47** (C3), 1-503 (1986)].
- V. Elser and C. L. Henley, *Phys. Rev. Lett.* **55**, 2883 (1985); C. L. Henley and V. Elser, *Philos. Mag. Lett.* **B53**, L59 (1986); P. Guyot and M. Audier, *Philos. Mag.* **B52**, L15 (1985); M. Audier and P. Guyot, *ibid.* **B53**, L43 (1986).
- P. Bak, *Phys. Rev. Lett.* **56**, 861 (1986); M. V. Jarić, *J. Phys. (Paris)* **47** (C3), 259 (1986).
- K. M. Knowles and W. M. Stobbs, *Nature (London)* **323**, 313 (1986).
- Y. Shen, S. J. Poon, W. Dmowski, T. Egami, G. J. Shiflet, *Phys. Rev. Lett.* **58**, 1440 (1987).
- P. A. Bancel, P. A. Heiney, P. W. Stephens, A. I. Goldman, P. M. Horn, *ibid.* **54**, 2422 (1985).
- P. M. Horn, W. Malzfeldt, D. P. DiVincenzo, J. Toner, R. Gambino, *ibid.* **57**, 1444 (1986).
- R. L. Robertson, M. E. Misener, S. C. Moss, L. A. Bendersky, *Acta Metall.* **34**, 2177 (1986).
- For an introduction to phasons, see P. Bak, *Rep. Prog. Phys.* **45**, 587 (1982); P. A. Kalugin, A. Yu Kitayev, L. S. Levitov, *J. Phys. (Paris)* **46**, L601 (1985).
- T. C. Lubensky *et al.*, *Phys. Rev. Lett.* **57**, 1440 (1986).
- J. E. S. Socolar *et al.*, *Phys. Rev. B* **34**, 3345 (1986).
- D. Shechtman and I. Blech, *Metal. Trans.* **B16**, 1005 (1985); P. W. Stephens and A. I. Goldman, *Phys. Rev. Lett.* **56**, 1168 (1986).
- J. W. Cahn and D. Gratias, *J. Phys. (Paris)* **47** (C3), 415 (1986); Y. Ma *et al.*, *Phys. Rev. Lett.* **57**, 1611 (1986); Y. Ma *et al.*, *ibid.*, p. 1956.
- E. R. Ryba, *Earth Miner. Sci.* **55**, 51 (1986); C. Bartges, M. H. Tosten, P. R. Howell, E. R. Ryba, *J. Mater. Sci.* **22**, 1663 (1987); P. Sainfort and B. Dubost, *J. Phys. (Paris)* **47** (C3), 321 (1986); B. Dubost, J. M. Lang, M. Tanaka, P. Sainfort, M. Audier, *Nature (London)* **324**, 48 (1986).
- F. W. Gayle, *J. Mater. Res.* **2**, 1 (1987).
- During the preparation of this manuscript we learned of a similar diffraction study of oriented grains of icosahedral Al-Mn prepared by ion implantation [J. D. Budai, J. Z. Tischler, A. Habenschuss, G. E. Ice, V. Elser, *Phys. Rev. Lett.* **58**, 2304 (1987)]. The results of this experiment were consistent with those reported here.
- The composition of a 245- μg crystallite with a minimum of impurity phases was determined by wet chemical analysis to be $\text{Al}_{5.8}\text{Li}_{2.7}\text{Cu}_{1.1}$; however, systematic variation of starting materials appeared to yield a maximum in icosahedral phase formation at a composition of $\text{Al}_{5.5}\text{Li}_{3.3}\text{Cu}_{1.1}$ in melt-spun ribbons.
- H. K. Hardy and J. M. Silcock, *J. Inst. Met.* **84**, 423 (1955).
- E. E. Cherkashin, P. I. Kripyakevich, G. I. Olskiv, *Sov. Phys. Crystallogr.* **8**, 681 (1964).
- C. Huyghens, *Traité de la lumière* (Paris, 1690) and R. J. Häüy, *Essai d'une théorie sur la structure des cristaux* (Paris, 1784).
- See, for example, J. F. Nye, *Physical Properties of Crystals: Their Representation by Tensors and Matrices* (Oxford Univ. Press, Oxford, U.K., 1957).
- The samples were first characterized and aligned on a precession camera by using $\text{Mo K}\alpha$ radiation. These studies confirmed the icosahedral symmetry of $\text{Al}_6\text{Li}_3\text{Cu}$ and are consistent with results reported elsewhere (16, 25). The samples were then mounted on a Huber four circle diffractometer at beamline X-20C at the National Synchrotron Light Source. A pair of asymmetrically cut Ge(111) monochromatic crystals tuned to 1.276 Å, and a flat Ge(111) analyzer crystal after the sample, produced an incident flux of 4×10^{11} photons per second into a 1-mm² spot at the sample and produced a longitudinal resolution of 4×10^{-4} Å⁻¹.
- A. R. Kortan *et al.*, *J. Mater. Res.* **2**, 294 (1987).
- P. A. Bancel and P. A. Heiney, *J. Phys. (Paris)* **47** (C3), 341 (1986).
- J. E. S. Socolar and D. C. Wright, *Phys. Rev. Lett.* **59**, 221 (1987).
- A. I. Goldman and P. W. Stephens, unpublished data.
- V. Elser, *Proceedings of the 15th International Colloquium in Physics*, R. Gilmore and D. H. Feng, Eds. (World Scientific, Singapore, in press), vol. 1.
- D. Levine *et al.*, *Phys. Rev. Lett.* **54**, 1520 (1985).
- D. Levine and A. Garg, unpublished data.
- T. L. Ho *et al.*, unpublished data.
- S. Sachdev and D. R. Nelson, *Phys. Rev. B* **32**, 4592 (1985).
- M. V. Jarić, *ibid.* **34**, 4685 (1986).
- We thank P. J. Steinhardt, J. S. Socolar, D. Wright, D. DiVincenzo, and J. Toner for useful conversations. P.A.B. and P.A.H. were supported by the National Science Foundation, grant no. DMR83-51063. Synchrotron beam line X-20C is supported in part by MIT Materials Research Laboratory under National Science Foundation grant DMR84-18718. The National Synchrotron Light Source, Brookhaven National Laboratory, is supported by the U.S. Department of Energy, Division of Materials Sciences and Division of Chemical Sciences.

21 May 1987; accepted 28 July 1987